

Modeling Na clusters in Ar matrices

F. Fehrer¹, M. Mundt^{1,2}, P.-G. Reinhard^{1,2}, and E. Suraud²

¹ Institut für Theoretische Physik, Universität Erlangen, Staudtstrasse 7, D-91058 Erlangen, Germany

² Laboratoire de Physique Théorique, Université Paul Sabatier, 118 Route de Narbonne, F-31062 Toulouse, cedex, France

We present a microscopic model for Na clusters embedded in raregas matrices. The valence electrons of the Na cluster are described by time-dependent density-functional theory at the level of the local-density approximation (LDA). Particular attention is paid to the semi-classical picture in terms of Vlasov-LDA. The Na ions and Ar atoms are handled as classical particles whereby the Ar atoms carry two degrees of freedom, position and dipole polarization. The interaction between Na ions and electrons is mediated through local pseudo-potentials. The coupling to the Ar atoms is described by (long-range) polarization potentials and (short-range) repulsive cores. The ingredients are taken from elsewhere developed standards. A final fine-tuning is performed using the NaAr molecule as benchmark. The model is then applied to embedded systems Na_8Ar_N . By close comparison with quantum-mechanical results, we explore the capability of the Vlasov-LDA to describe such embedded clusters. We show that one can obtain a reasonable description by appropriate adjustments in the fine-tuning phase of the model.

Copyright line will be provided by the publisher

1 Introduction

Structure and dynamics of metal clusters has been a much studied topic over the last two decades, see e.g. [1, 2, 3]. While optical response was in the focus of numerous earlier studies, recent developments aim at exploring cluster dynamics in all its aspects [4]. The preferred theoretical tool for describing clusters in all dynamical regimes is the time-dependent local-density approximation (TDLDA) which treats the cluster electrons at a fully quantum mechanical level, however in an independent-particle picture as motion in a common self-consistent mean-field. For highly excited systems, one can employ a semi-classical approximation in terms of phase-space dynamics described by the Vlasov equation, in the cluster context called a Vlasov-LDA. The Vlasov equation was originally used in a genuinely classical environment for plasma physics [5]. Nuclear physicists have adapted it to finite quantum systems for the description of violent heavy-ion collisions [6]. The motivation is twofold: first, the Vlasov description becomes more efficient for highly excited system, and second, the semi-classical approach makes it feasible to include correlations simply in terms of an Ühling-Uhlenbeck collision term (extended Vlasov to VUU). The successful applications in nuclear dynamics have motivated the transfer of the method to cluster physics, in the first round using a jellium model for the ionic background [7, 8, 9] but later also in connection with detailed ions [10, 11]. These applications of Vlasov-LDA and VUU dealt up to now only with free metal clusters. Many experiments, however, are done on supported or embedded clusters, see for example the study of the systematics of optical properties in small Ag clusters [12]. There is thus a need to develop reliable and efficient models for the cluster-substrate interface in connection with cluster dynamics in various regimes. Such developments are underway for TDLDA in embedded clusters whereby raregas matrices are considered as a substrate with simple constituents [13, 14, 15]. They take up the modeling of the Ar atoms and their interaction with the Na cluster from earlier quantum-chemical considerations [16]. It is the aim of the present paper to investigate the performance of Vlasov-LDA and VUU for metal clusters embedded in raregas matrices. To that end, we recycle the interface model from the TDLDA studies and combine it with the Vlasov-LDA description for the cluster electrons. We intend to develop a parameterization of the model which provides acceptable ground state structures. These are then used as laboratory for dynamical studies.

Copyright line will be provided by the publisher

electrons	\longleftrightarrow	$\{\varphi_n(\mathbf{r}), n = 1 \dots N_{\text{el}}\}$	\implies	$f(\mathbf{r}, \mathbf{p})$
cluster ions	\longleftrightarrow	$\{\mathbf{R}_I, I = 1 \dots N_{\text{ion}}\}$		
Ar core	\longleftrightarrow	$\{\mathbf{R}_a, a = 1 \dots N_{\text{Ar}}\}$		
Ar valence cloud	\longleftrightarrow	$\mathbf{R}'_a = \mathbf{R}_a + \mathbf{s}_a$		

Table 1 Short summary of the degrees of freedom of the model. Note that the center of the valence cloud \mathbf{R}'_a serves to characterize the Ar dipole moment through $\mathbf{d} = eq_{\text{Ar}}\mathbf{s} = eq_{\text{Ar}}(\mathbf{R}' - \mathbf{R})$ where q_{Ar} is the net charge of the valence cloud.

In the first exploration here, we use a simple excitation mechanism (instantaneous boost) to evaluate the basic features of dynamical response in various regimes, namely spectral distributions and ionization. The validity and limitations of Vlasov-LDA are scrutinized by comparison with results from quantum mechanical TDLDA. We also exploit the option of VUU for a first exploration of dynamical correlations and their interplay with the substrate.

The paper is outlined as follows: In section 2, we present the model in detail thereby providing all information for full TDLDA as well as for the semi-classical approaches. In section 3, we summarize briefly the emerging equations of motion and their numerical solution. In section 4, we discuss the calibration of the model using the NaAr molecule as benchmark. Finally in section 5, we present and discuss first results for an embedded cluster with Na_8Ar_N as test cases.

2 The Na-Ar energy functional in detail

2.1 The degrees of freedom

The key constituents are the valence electrons of the metal cluster. Starting point for their description is quantum mechanical mean-field theory where each electron is associated with one single-particle wavefunction $\{\varphi_n(\mathbf{r}), n = 1 \dots N_{\text{el}}\}$. The φ_n are determined by a (time-dependent) Kohn-Sham equation. The manifold of occupied wavefunctions is comprised in the one-electron density matrix $\rho(\mathbf{r}, \mathbf{r}') = \sum_n \varphi_n(\mathbf{r})\varphi_n^\dagger(\mathbf{r}')$. We perform a semi-classical approximation in order to obtain a description in terms of the one-electron phase-space distribution $f(\mathbf{r}, \mathbf{p})$ [17]. This yields the Vlasov-LDA which has shown to provide a reliable description of dynamical processes in free metal clusters with detailed ionic structure [18, 19]. The other ingredients are the Na ions in the cluster and the raregas atoms. They are treated by classical molecular dynamics in terms of positions \mathbf{R} and associated momenta \mathbf{P} . The Ar atom carries as internal degree of freedom a dipole moment to account for the polarization interaction. Effective Ar potentials for static calculations contain that implicitly. True dynamics requires explicit dipoles as we use it here. It is convenient to formulate the Ar dipoles \mathbf{d}_a in terms of the displacement $\mathbf{R}'_a - \mathbf{R}_a = \mathbf{d}_a/eq_{\text{Ar}}$. All these degrees of freedom are summarized in table 1.

The detailed description of the Ar atoms is outlined in the next subsection 2.2. What the Na^+ ions is concerned, we neglect the small dipole polarizability of the Na^+ core and treat it merely as a monopole. The ions are taken as point charges in the interaction with the Ar atoms. Soft and local pseudo-potentials are used for the interaction with the cluster electrons [20], see eq. (5). The density of the electrons is given naturally as defined in mean-field theories. It reads in the quantum mechanical version

$$\rho_{\text{el}}(\mathbf{r}) = \sum_{\alpha} |\varphi_{\alpha}(\mathbf{r})|^2 \quad (1a)$$

and in Vlasov-LDA

$$\rho_{\text{el}}(\mathbf{r}) = \int d^3p f(\mathbf{r}, \mathbf{p}) \quad . \quad (1b)$$

2.2 Construction of soft dipole potentials

A finite dipole momentum in Ar atom is generated from Coulomb fields of the other constituents or from the excitation mechanism. In turn, it produces a dipole field to the outside world. However, a pure dipole field has a huge singularity at the origin. This is unphysical because we are not having point dipoles in practice. With a closer look at the Ar atom we see that the dipole is generated from a deformation (more precisely, displacement) of the outer electron shell (*3s-3p*-shell) and the finite size of the source delivers regular Coulomb fields everywhere. We thus specify the dipole momentum of the Ar atom in more detail. The Ar atom is thought of consisting out of a valence electron cloud with center of mass \mathbf{R}'_a and of the corresponding positively charged core placed at the atom position \mathbf{R}_a . (In fact, one should use the center-of-mass of core plus valence cloud but the recoil effect on the Ar core is negligible, thus neglected). Both, valence cloud and core have the same absolute value of charge q_{Ar} delivering together a neutral atom. A small displacement of the valence electrons against the core produces a net dipole moment. The profile of valence cloud and core is described by the same Gaussian with width σ_{Ar} , yielding together the charge distribution of one Ar atom as

$$\rho_{\text{Ar},a}(\mathbf{r}) = \frac{eq_{\text{Ar}}}{\pi^{3/2}\sigma_{\text{Ar}}^3} \left[\exp\left(-\frac{(\mathbf{r}-\mathbf{R}_a)^2}{\sigma_{\text{Ar}}^2}\right) - \exp\left(-\frac{(\mathbf{r}-\mathbf{R}'_a)^2}{\sigma_{\text{Ar}}^2}\right) \right] \quad (2a)$$

where the index a stands for Ar atom number a implying atom position \mathbf{R}_a and valence cloud \mathbf{R}'_a . The Coulomb potential of this charge density produces the polarization-part of the potential exerted from the Ar atoms,

$$V_{\text{Ar},a}^{(\text{pol})}(\mathbf{r}) = e^2 q_{\text{Ar}} \left[\frac{\text{erf}(|\mathbf{r}-\mathbf{R}_a|/\sigma_{\text{Ar}})}{|\mathbf{r}-\mathbf{R}_a|} - \frac{\text{erf}(|\mathbf{r}-\mathbf{R}'_a|/\sigma_{\text{Ar}})}{|\mathbf{r}-\mathbf{R}'_a|} \right], \quad (2b)$$

where q_{Ar} is the effective charge of the Ar cloud and core (see below). The error function therein is defined as

$$\text{erf}(r) = \frac{2}{\sqrt{\pi}} \int_0^r dx e^{-x^2}. \quad (2c)$$

2.3 The total energy

The model is fully specified by giving the total energy of the system. It is composed as

$$E_{\text{total}} = \underbrace{E_{\text{Na,el}} + E_{\text{Na,ion}} + E_{\text{ion,el}}}_{\text{Na cluster}} + E_{\text{Ar}} + E_{\text{coupl}} + E_{\text{vdW}}, \quad (3a)$$

$$E_{\text{Na,el}} = E_{\text{kin}} + E_{\text{Hartree}}(\rho_{\text{el}}) + E_{\text{xc}}(\rho_{\text{el}}) + \int d\mathbf{r} V_{\text{ext}}(\mathbf{r}, t) \rho_{\text{el}}(\mathbf{r}) \quad , \quad (3b)$$

$$E_{\text{Na,ion}} = \sum_I \frac{\mathbf{P}_I^2}{2M_{\text{Na}}} + \sum_{I < J} \frac{e^2}{|\mathbf{R}_I - \mathbf{R}_J|} \quad , \quad (3c)$$

$$E_{\text{ion,el}} = \sum_I \int d\mathbf{r} V_{\text{PsP}}(|\mathbf{r} - \mathbf{R}_I|) \rho_{\text{el}}(\mathbf{r}) \quad , \quad (3d)$$

$$\begin{aligned} E_{\text{Ar}} = & \sum_a \frac{\mathbf{P}_a^2}{2M_{\text{Ar}}} + \sum_a \frac{\mathbf{P}'_a{}^2}{2m_{\text{Ar}}} + \frac{1}{2} k_{\text{Ar}} (\mathbf{R}'_a - \mathbf{R}_a)^2 \\ & + \sum_{a < a'} \left[\int d\mathbf{r} \rho_{\text{Ar},a}(\mathbf{r}) V_{\text{Ar},a'}^{(\text{pol})}(\mathbf{r}) + V_{\text{ArAr}}^{(\text{core})}(\mathbf{R}_a - \mathbf{R}_{a'}) \right] \\ & + \sum_a \int d\mathbf{r} V_{\text{ext}}(\mathbf{r}, t) \rho_{\text{Ar},a}(\mathbf{r}) \quad , \end{aligned} \quad (3e)$$

$$\begin{aligned} E_{\text{coupl}} = & \sum_{I,a} \left[V_{\text{Ar},a}^{(\text{pol})}(\mathbf{R}_I) + V'_{\text{NaAr}}(\mathbf{R}_I - \mathbf{R}_a) \right] \\ & + \int d\mathbf{r} \rho_{\text{el}}(\mathbf{r}) \sum_a \left[V_{\text{Ar},a}^{(\text{pol})}(\mathbf{r}) + W_{\text{elAr}}(|\mathbf{r} - \mathbf{R}_a|) \right] \quad , \end{aligned} \quad (3f)$$

$$E_{\text{VdW}} = e^2 \frac{1}{2} \sum_a \alpha_a \left[\frac{1}{N_{\text{el}}} \left(\int d\mathbf{r} \mathbf{f}_a(\mathbf{r}) \rho_{\text{el}}(\mathbf{r}) \right)^2 - \int d\mathbf{r} \mathbf{f}_a(\mathbf{r})^2 \rho_{\text{el}}(\mathbf{r}) \right] \quad , \quad (3g)$$

$$\mathbf{f}_a(\mathbf{r}) = \nabla \frac{\text{erf}(|\mathbf{r} - \mathbf{R}_a|/\sigma_{\text{Ar}})}{|\mathbf{r} - \mathbf{R}_a|} \quad . \quad (3h)$$

The electronic kinetic energy depends on the level of approach, i.e.

$$E_{\text{kin}} = \sum_n |\nabla \varphi_n|^2 \quad (3i)$$

in the quantum case and

$$E_{\text{kin}} = \int d^3p \frac{\mathbf{p}^2}{2m_{\text{el}}} f(\mathbf{r}, \mathbf{p}) \quad . \quad (3j)$$

in the Vlasov case. The Van-der-Waals energy E_{VdW} is a correlation from the dipole excitation in the Ar atom coupled with a dipole excitation in the cluster. It requires, in principle, an energy denominator involving the basic excitation energy ΔE_{Ar} in the Ar atom and the typical excitation energy in the Na cluster which is $\approx \omega_{\text{Mie}}$. We exploit the fact that $\omega_{\text{Mie}} \ll \Delta E_{\text{Ar}}$ and eliminate the energy denominator in the spirit of a closure approximation. This amounts to compute the variance of the dipole operator in the cluster. It employs, in fact, an effective dipole operator \mathbf{f}_a , see eq. (3h), which corresponds to the dipole field from the smoothed Ar charge distributions. The dipole variance as expectation value within the many-body wavefunctions is, furthermore, simplified in terms of the local variance. This yields finally the approximation (3g) to the Van-der-Waals energy. Its computation is still very cumbersome. It becomes particularly involved in the semi-classical case. On the other hand, Vlasov-LDA is intended for the regime of high excitations where subtle details, as e.g. the Van-der-Waals force do not matter. Thus we skip E_{VdW} in Vlasov-LDA.

It is obvious that the polarization potentials are handled in terms of effective smoothed pseudo-densities (2a) and their resulting Coulomb potential (2b). The repulsive core potentials require explicit

modeling. We take it mainly from literature. The contributions are

$$W_{\text{elAr}}(r) = e^2 \frac{A_{\text{el}}}{1 + e^{\beta_{\text{el}}(r-r_{\text{el}})}} \quad (4a)$$

$$V_{\text{ArAr}}^{(\text{core})}(R) = e^2 1.367 \cdot 10^{-3} \left[\left(\frac{6.501}{R} \right)^{12} - \left(\frac{6.501}{R} \right)^6 \right] \quad (4b)$$

$$V'_{\text{ArNa}}(R) = e^2 \left[A_{\text{Na}} \frac{e^{-\beta_{\text{Na}}R}}{R} - \frac{2}{1 + e^{\alpha_{\text{Na}}/R}} \left(\frac{C_{\text{Na},6}}{R^6} + \frac{C_{\text{Na},8}}{R^8} \right) \right] \quad (4c)$$

	β_{Na}	α_{Na}	A_{Na}	$C_{\text{Na},6}$	$C_{\text{Na},8}$
quantum mechanical LDA	1.7624 a_0^{-1}	1.815 a_0	334.85 Ha	52.5 Ha a_0^6	1383 Ha a_0^8
Vlasov-LDA	1.670 a_0^{-1}	5.6 a_0	242.32 Ha	225 Ha a_0^6	4410 Ha a_0^8

Table 2 Parameters for the ion-Ar pseudo-potential in Na according to the form (4c).

For the Ar-Ar core interaction we employ a Lennard-Jones type potential with parameters such that binding properties of bulk Ar are reproduced. The Na-Ar core potential has been fitted according to [21]. Note that the Na-Ar potential from [21] does contain also a long range part $\propto \alpha_{\text{Ar}}$ which accounts for the dipole polarization-potential. We describe that long range part explicitly and have to omit it here. We thus choose the form (4c). The pseudo-potential W_{elAr} for the electron-Ar core repulsion has been modeled according to the proposal of [16]. Its parameters will be re-tuned as discussed below.

2.4 The ion-electron pseudo-potential

The pseudo-potential for the coupling (3d) between Na ions and electrons is taken in a soft and local form as [20]

$$V_{\text{PsP}}(r) = -\frac{e^2}{r} \left[c_1 \text{erf} \left(\frac{r}{\sqrt{2}\sigma_1} \right) + c_2 \text{erf} \left(\frac{r}{\sqrt{2}\sigma_2} \right) \right] \quad (5)$$

with the error function given in eq. (2c). The parameters were adjusted to the properties of Na atom and bulk. This serves to provide simultaneously correct bond lengths for Na molecule and clusters as well as as good description of optical response, all in the framework of quantum-mechanical (TD)LDA [20]. A semi-classical description of Na clusters does also work very well with a pseudo-potential in the form (5). But it requires a new adjustment of the parameters suited for the Vlasov approach [22]. Both version for the parameters are summarized in table 3.

2.5 The parameters for the polarization potential

The polarizability of the Ar atoms is described by the model of a rigid cloud of valence electrons which is oscillating against the remaining raregas ion. The parameters of the model are:

	c_1	c_2	σ_1	σ_2
quantum mechanical LDA	-2.29151	3.29151	0.681 a_0	1.163 a_0
Vlasov-LDA	-0.5	1.5	0.7778 a_0	1.5556 a_0

Table 3 Parameters for the ion-electron pseudo-potential in Na according to the local form (5). Different sets are to be used for quantum mechanical LDA and for semi-classical Vlasov-LDA.

binding distance d_0	$9.5 a_0$
depth E_0 of the $X^2\Sigma^+$ ground-state	44 cm^{-1}
energy of the transition $X^2\Sigma^+ \rightarrow B^2\Sigma^+$	0.155 Ry

Table 4 Basic properties of the NaAr molecule as they are used for fine tuning the model parameters.

$$\begin{aligned} q_{\text{Ar}} &= \text{effective charge of valence cloud} \\ m_{\text{Ar}} &= \text{effective mass of valence cloud} \\ k_{\text{Ar}} &= \text{restoring force for dipoles} \end{aligned}$$

These parameters are adjusted to reproduce the basic response properties of the raregas atom in the low energy domain, i.e. we choose to reproduce the static polarizability α_{RG} and the second derivative of the dynamical polarizability $\partial_\omega^2 \alpha_D|_{\omega=0}$. To that end, we make a one-pole model having the dispersion relation

$$\alpha_{\text{Ar}}(\omega) = \frac{\alpha_{\text{Ar}}(0)}{1 - \frac{\omega^2}{\omega_0^2}} \approx \alpha_{\text{Ar}} + \frac{\alpha_{\text{Ar}}}{\omega_0^2} \omega^2 \quad . \quad (6a)$$

The frequency, in turn, is related to spring constant and mass as usual

$$\omega_0 = \sqrt{k_{\text{Ar}}/m_{\text{Ar}}} \quad .$$

On the other hand, the spring constant is directly related to the static polarizability as

$$k_{\text{Ar}} = \frac{e^2 q_{\text{Ar}}^2}{\alpha_{\text{Ar}}} \quad . \quad (6b)$$

We identify the mass of the electron cloud with its charge and the electron mass as

$$m_{\text{Ar}} = q_{\text{Ar}} m_{\text{el}} \quad . \quad (6c)$$

thus we find for the effective charge of the valence cloud

$$q_{\text{Ar}} = \frac{\alpha_{\text{Ar}} m_{\text{el}} \omega_0^2}{e^2} \quad . \quad (6d)$$

The folding width of the valence cloud is determined such that the restoring force from the folded Coulomb (for small displacements) reproduces the spring constant k_{Ar} . This yields

$$\sigma_{\text{RG}} = \left(\alpha_{\text{Ar}} \frac{4\pi}{3(2\pi)^{3/2}} \right)^{1/3} \quad . \quad (6e)$$

For Ar we use

$$\alpha_{\text{Ar}}(0) = 11.08 a_0^3 \quad , \quad \omega_0 = 1.755 \text{ Ry} \quad . \quad (6f)$$

The eqs. (6) determine the parameters for the polarization potentials at the side of the Ar atoms.

2.6 Fine tuning of electron-Ar core potential

The parameters of the electron-Ar core potential (4a) determine sensitively the binding properties of Na to the Ar atoms. We use that potential as a means for a final fine-tuning of the model. The benchmark for adjustment is provided by the Na-Ar dimer. The data are taken from [23] and [24] and summarized in table 4. There are three data points and three parameters to be adjusted, namely A_{el} , β_{el} , and r_{el} . It turns out that these three parameters compensate each other to some extent. One can, e.g. vary the potential height A_{el} and obtain about the same fit with re-tuning the other two parameters. Fortunately, we find a reasonable fit to the wanted data in spite of that restricted flexibility. Moreover, we exploit the freedom in the choice of A_{el} to produce the softest reasonable core potential. It is obvious that such a subtle adjustment depends crucially on the level of approach. We thus obtain two different sets for quantum calculation and for Vlasov LDA, similar as it was the case already for the Na ion-electron pseudo-potential. The final parameters are summarized in table 5.

	A_{el}	β_{el}	r_{el}
quantum mechanical LDA	0.47	1.6941/ a_0	2.2 a_0
Vlasov-LDA	0.4	1.44 / a_0	1.8 a_0

Table 5 Parameters for the ion-electron pseudo-potential in Na according to the local form (5). Different sets are to be used for quantum mechanical LDA and for semi-classical Vlasov-LDA.

3 Dynamical equations and their solution

3.1 The equations of motion

The energy functional once specified (see section 2) determines structure and dynamics of the coupled system. This follows standard techniques throughout. We thus give here only a very brief summary. More details can be found in [4, 4] and specifically for the semi-classical approach in [9, 18].

The equations of motion are determined variationally. They read

$$i\partial_t\varphi_n = \left(\frac{\hat{\mathbf{p}}^2}{2m_{\text{el}}} + U_{\text{KS}} \right) \varphi_n \quad , \quad (7a)$$

$$U_{\text{KS}}(\mathbf{r}) = \frac{\delta E_{\text{total}}}{\delta \rho_{\text{el}}(\mathbf{r})} \quad , \quad (7b)$$

$$\partial_t \mathbf{R} = \nabla_{\mathbf{P}} E_{\text{total}} \quad , \quad \partial_t \mathbf{P} = -\nabla_{\mathbf{R}} E_{\text{total}} \quad , \quad \mathbf{R} \in \{\mathbf{R}_I, \mathbf{R}_a, \mathbf{R}'_I\} \quad , \quad (7c)$$

for the case of quantum-mechanical propagation of electrons. Only eq. (7a) is to be replaced by the Vlasov equation for the phase-space distribution $f(\mathbf{r}, \mathbf{p}, t)$, i.e.

$$\partial_t f + \left\{ \frac{\hat{\mathbf{p}}^2}{2m_{\text{el}}} + U_{\text{KS}}, f \right\} = 0 \quad (7d)$$

where $\{\dots, \dots\}$ is the classical Poisson bracket. Note that the self-consistent Kohn-Sham potential U_{KS} using the LDA energy functional is employed. That is why the scheme is called Vlasov-LDA. In fact, the above equations of motion describe electronic dynamics, in terms of TDLDA or Vlasov-LDA, coupled to classical MD for ions and atoms. The whole scheme is then TDLDA-MD in the quantum case or Vlasov-LDA-MD in the semi-classical approximation.

It is the great advantage of the semi-classical approximation that it allows to include dynamical electronic correlations through an Ühling-Uhlenbeck collision term. This extends Vlasov-LDA to the Vlasov-Ühling-Uhlenbeck scheme (VUU). The eq. (7d) is then extended to

$$\partial_t f + \left\{ \frac{\hat{\mathbf{p}}^2}{2m_{\text{el}}} + U_{\text{KS}}, f \right\} = I_{\text{UU}} \quad , \quad (7e)$$

$$I_{\text{UU}}(\mathbf{r}, \mathbf{p}_1, t) = \int d^3 p_2 d^3 p_3 d^3 p_4 W(12, 34) (f_{1,2}^{\text{out}} f_{3,4}^{\text{in}} - f_{1,2}^{\text{in}} f_{3,4}^{\text{out}}) \quad , \quad (7f)$$

$$W(12, 34) = \frac{1}{m_{\text{el}}^2} \frac{d\sigma}{d\omega} \delta(\mathbf{p}_1 + \mathbf{p}_2 - \mathbf{p}_3 - \mathbf{p}_4) \delta(E_1 + E_2 - E_3 - E_4) \quad , \quad (7g)$$

$$f_{i,j}^{\text{in}} = f(\mathbf{r}, \mathbf{p}_i, t) f(\mathbf{r}, \mathbf{p}_j, t) \quad , \quad (7h)$$

$$f_{k,l}^{\text{out}} = (1 - (2\pi\hbar)^3 \frac{f(\mathbf{r}, \mathbf{p}_k, t)}{2}) (1 - (2\pi\hbar)^3 \frac{f(\mathbf{r}, \mathbf{p}_l, t)}{2}) \quad , \quad (7i)$$

where $i \equiv (\mathbf{r}, \mathbf{p})$ is used as an abbreviation and $d\sigma/d\omega$ is the in-medium electron-electron cross section. We use here the cross section which had been evaluated for Na clusters [9, 18].

The numerical solution of the coupled equations of motion employs different methods for the different ingredients [25]. The quantum-mechanical Kohn-Sham equation (7a) is solved by the time-splitting

method [26]. The classical MD (7c) for ions and atoms is propagated by the (velocity) Verlet algorithm [27]. The handling of the Vlasov equation (7d) and associated collision term (7f-7i) is more involved. It will be detailed in the next subsection 3.2.

The static solution has to be provided before any dynamics can take off. The ionic/atomic configuration is found by a mix of simulated annealing and direct gradient towards the energy minimum. Standard methods for the stationary Kohn-Sham equation apply in case of the quantum mechanical treatment. Most involved is again the semi-classical case. A stable ground state distribution $f_0(\mathbf{r}, \mathbf{p})$ for the Vlasov equation is determined by the Thomas-Fermi method [9, 18]. It is to be noted that the density and mean field entering Thomas-Fermi has to be properly augmented with the test-particle folding (see next section) in order to produce consistent input for the Vlasov solution with the test-particle method.

3.2 Test particle method

The phase-space distribution is a function in six-dimensional phase space. Its representation on a (six-dimensional) grid is even today beyond the capacity of computers. One thus uses a representation in terms of test-particles. This technique had been imported for cluster physics from the well developed nuclear physics case [6]. The smooth one-body phase-space distribution f is represented by a swarm of pseudo-particles each one having a certain width, i.e.

$$f(\mathbf{r}, \mathbf{p}, t) = \frac{N_{\text{el}}}{N_{\text{PP}}} \sum_{i=1}^{N_{\text{PP}}} g_r(\mathbf{r} - \mathbf{r}_i(t)) g_p(\mathbf{p} - \mathbf{p}_i(t)) \quad , \quad (8a)$$

$$g_x(\mathbf{x}) = (2\pi\sigma_x^2)^{-3/2} \exp\left(-\frac{\mathbf{x}^2}{2\sigma_x^2}\right) \quad , \quad x \in \{r, p\} \quad , \quad (8b)$$

$$\sigma_r \sigma_p = \hbar \quad , \quad (8c)$$

$$\sigma_r = 1.7836 a_0 \quad . \quad (8d)$$

The folding widths σ_r and σ_p are free parameters of the method. Relation (8c) is connected to the Husimi picture [28] which gives the elementary distribution $g_r g_p$ the interpretation of a minimal quantum-mechanical wavepacket being used as means to derive and justify the semi-classical limit in the smoothest way [17, 29, 30]. There remains σ_r as free parameter. It can be used to accommodate quantum-mechanical binding properties through the Vlasov approximation as good as possible and it has been used successfully that way for free clusters in jellium approach [7, 8, 9] as well as with detailed ionic background [10, 11, 18]. We use the value (8d) which provides a good reproduction of free neutral Na clusters.

Inserting the ansatz (8) into the Vlasov equation (7d) yields the following equation of motion for the test particles

$$\partial_t \mathbf{r}_i(t) = \mathbf{p}_i / m_{\text{el}} \quad , \quad (9a)$$

$$\partial_t \mathbf{p}_i(t) = -\nabla_{\mathbf{r}_i} U_{\text{KS},g} \quad , \quad (9b)$$

$$U_{\text{KS},g} = g_r \star U_{\text{KS}} = \int d^3 r' g_r(\mathbf{r} - \mathbf{r}') U_{\text{KS}}(\mathbf{r}') \quad . \quad (9c)$$

The Kohn-Sham potential is obtained from the ionic/atomic positions and the actual electron density computed with eq. (1b) which reads in the test-particle representation

$$\rho_{\text{el}}(\mathbf{r}, t) = \frac{N_{\text{el}}}{N_{\text{PP}}} \sum_{i=1}^{N_{\text{PP}}} g_r(\mathbf{r} - \mathbf{r}_i(t)) \quad . \quad (9d)$$

Note that the g_r folded Kohn-Sham potential (9c) is employed in the test-particle propagation (9b). This complies with the Husimi picture and it allows an efficient handling of density and mean-field on a spatial coordinate-space grid. The density is accumulated on the grid with eq. (9d) using the g_r so to say as

interpolation functions. The Coulomb and exchange-correlation potentials are determined on the grid composing the Kohn-Sham potential together with the potentials from ions and atoms. The forces on the test-particle are retrieved from the grid again with the help of the folding functions g_r . This is the practical side of eq. (9c).

The finite representation in terms of test-particles induces a principle long-time instability towards a final Boltzmann equilibrium distribution. This is unphysical because it violates the Pauli principle [31, 32]. The critical time depends on folding width and number of test particles. The folding width is fixed by the adjustment to quantum features. It remains the particle number. We chose $N_{tp} = 4000$ per electron. This provides sufficient stability over the time scale considered (200 fs). The collision term (7f) in VUU contains the Pauli blocking. This provides long time stability of the propagation.

The practical evaluation of the collision term is already simplified by the test particle. The nine-fold momentum-space integration is replaced by four-fold summation over test-particles, each factor f_i contributing one sum. The scattering process connects two incoming momenta with two outgoing ones, $(\mathbf{p}_1, \mathbf{p}_2) \longrightarrow (\mathbf{p}_3, \mathbf{p}_4)$. The outgoing momenta are fixed by momentum and energy conservation laws up to a scattering angle. The scattering angle is chosen from the unit sphere at random.

3.3 Excitation mechanism and observables

Typical cluster excitations are promoted by laser pulses or collision with highly charged ions. Both can be described as external time-dependent Coulomb fields acting on the cluster. The coupling to the field $V_{\text{ext}}(\mathbf{r}, t)$ is provided for that purpose in the basic energy functional (3). A laser pulse, e.g., is characterized by $V_{\text{ext}} \propto \hat{D} \cos(\omega t) f_{\text{profile}}(t)$. In this first survey, we are interested mainly on general spectral properties. These are explored in the limiting case of an arbitrarily short laser pulse. It is realized by an instantaneous initial boost of the whole electron cloud which reads, in the Vlasov case,

$$f(\mathbf{r}, \mathbf{p}, t=0) = f_0(\mathbf{r}, \mathbf{p} + \mathbf{b}) \quad (10)$$

where f_0 is the ground state distribution and \mathbf{b} is the boost momentum. In the quantum case the boost is applied to each electron orbital as

$$\varphi_\alpha(\mathbf{r}) \longrightarrow \varphi_\alpha(\mathbf{r}, t=0) = e^{i\mathbf{b}\cdot\mathbf{r}} \varphi_\alpha(\mathbf{r}) \quad (11)$$

The size of \mathbf{b} determines the dynamical regime. Small \mathbf{b} explore the regime of linear response.

The dipole spectrum (optical absorption) is obtained from the subsequent dipole signal $\mathbf{D}(t) = \int d^3r \rho_{\text{el}}(\mathbf{r}, t) \mathbf{e}\mathbf{r}$. It is recorded over the whole time evolution. The dipole strength is finally obtained from the imaginary part of the Fourier transform, $\Im\{\hat{\mathbf{D}}(\omega)\}$. The three vector components correspond to the modes in x -, y -, and z -direction. For details see [4, 25, 33].

A further key observable is electron emission. The computation of the number of emitted electrons N_{esc} is straightforward. In TDLDA, we use absorbing boundary conditions [25]. The lost electrons are determined as the complement of the still remaining electrons $N_{\text{esc}} = N(0) - \int d^3r \rho_{\text{el}}(\mathbf{r}, t)$. In Vlasov-LDA, we draw a large sphere around the simulation area with radius $20 a_0$ and count explicitly all test-particles leaving that sphere.

4 Benchmark NaAr

Most of the parameters entering our model are taken from other grounds, i.e. from values published elsewhere and adjusted to independent data. The various constituents contribute strongly counteracting forces. This calls for some freedom to final fine-tuning. We exploit the anyway not so easily determined electron-Ar core potential for that purpose. The form (4a) is taken from quantum-chemical investigations [16]. The parameters are given free for fine-tuning. Thereby we consider the Na-Ar dimer as benchmark. The fully quantum mechanical TDLDA includes the Van-der-Waals interaction (3g) while the semi-classical

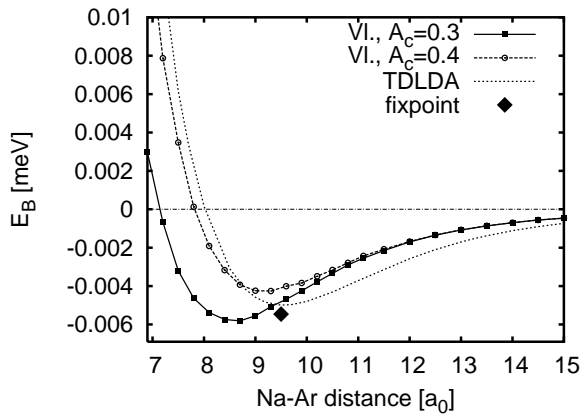


Fig. 1 The Born-Oppenheimer surface for the NaAr dimer computed semi-classically with the test-particle representation and compared with full TDLDA. The parameters for both TDLDA and semi-classics are given in table 5. In the semi-classical case, two different core heights in the Ar-electron core potential (4a) are considered. The value $A_c = 0.4$ is the final standard. The filled rhombus indicates the fitting point as listed in table 4.

approach does not have that term. The missing contribution is then mimicked to some extent by the readjustment of the free parameters of the electron-Ar potential. Figure 1 shows the Born-Oppenheimer surfaces for the Na-Ar molecule. The TDLDA fit complies nicely with the data point. The semi-classical results manage to reach that approximately. The results from two different core heights serve to demonstrate the variances one can explore in the adjustment: while reducing the core height, one can shift the minimum closer to the wanted value, but at the same time one finds the bonding energy moving off the optimum. Whatever one does, one finds that the semi-classical Born-Oppenheimer surfaces fall off much more quickly than the TDLDA one. Note that the asymptotic in case of TDLDA is dominated by the Van-der-Waals attraction $\propto r^{-6}$. Vlasov-LDA does not have that term and thus is bound to display a different asymptotics. Altogether, one sees that it is by no means trivial that a good adjustment can be found at all. Thus the TDLDA fit is a remarkable agreement and we are also satisfied with the semi-classical results which manage to find a fair agreement for the binding point. One has to keep in mind that the stronghold of Vlasov-LDA and VUU are the energetic processes. For these it suffices to provide a stable starting ground-state configuration which reproduces roughly realistic binding properties. This is achieved by the choice of parameters as listed in table 5. Thereby we have preferred the larger core height which provides the correct bond length while giving a slightly too small binding energy. Note that the semi-classical adjustment was done without explicit Van-der-Waals energy. This term is derived from quantum mechanical perturbation theory. Its implementation in a semi-classical environment requires deeper theoretical development and what we have found would increase the computational cost by an order of magnitude. That is not very useful for an approach which concentrates on processes far above the low energy scale of binding.

A further benchmark point for TDLDA is the energy for the $X^2\Sigma^+ \rightarrow B^2\Sigma^+$ transition at the bonding configuration. The goal is a transition energy of 0.155 Ry (see table 5); the TDLDA result with the optimized parameters is 0.164 Ry, a satisfying agreement. This benchmark cannot be applied for the semi-classical approach because there are no quantized single-particle states and thus no specific transitional energy spectra. We will apply Vlasov-LDA to metal clusters. These have the Mie surface plasmon as prominent excitation mode and this mode is determined by collective flow rather than by single-particle excitations. Thus we can expect a good reproduction of the Mie plasmon in spite of the missing single-particle adjustment. This is indeed the case as many previous applications for free metal clusters have exemplified [7, 8, 9, 10, 18, 11]. We have yet to see how the model performs for embedded clusters.

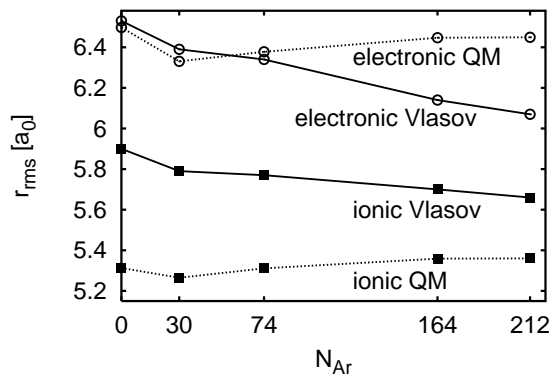


Fig. 2 Ionic and electronic radii of a Na_8 cluster embedded in Ar matrices of different size. Results from Vlasov and from quantum mechanical treatment are compared.

5 The Na_8Ar_N system

5.1 Structure

The ground state configurations involve 8–220 ions and atoms. This is hard to visualize in all detail. The basic structure, however, is simple [13, 14]. There exist three close isomers for the Na_8 clusters [14]. We consider here the Na_8 cluster in the shape consisting out of two rings with each four electrons. The Ar matrix was originally arranged in radial shells. It is slightly perturbed by the embedded cluster. But the shells still remain a useful guide and sorting scheme. Thus we will characterize the Na_8 cluster by its global root-mean-square radius and the Ar matrix is visualized as distribution of atoms in radial shells.

Figure 2 shows the radii for the (embedded) Na_8 . The ionic radii are generally smaller than the electronic ones because the electronic cloud reaches farther out than the well localized ions. The difference between electronic and ionic radius is caused mainly by the Gaussian folding with width σ_r . It is thus nearly constant. It is of the same order (although somewhat smaller) as the difference for the quantum mechanical case. The latter shows an interesting detail: it is practically constant for cases with Ar matrix but jumps by $0.2 a_0$ for the free cluster. This is due to the onset of core repulsion, similar as the first step for Vlasov LDA. In the further evolution, the radii show a different trend. While they slowly grow with N_{Ar} in the quantum mechanical case, they shrink for Vlasov-LDA. This hints at a different mix of interactions with the Ar atoms. The Ar core repulsion is felt more strongly for the test-particle in Vlasov-LDA because these are associated rigidly with a Gaussian distribution. The repulsive core wants to push away the tail and thus pushes the whole Gaussian. This works much different for the quantum mechanical case. The electron cloud can react more “elastically”. It allows for a dip near the Ar core and evolves else-wise almost unperturbed around it. Thus the dipole attraction can act more freely to pull the electronic tail outward.

Figure 3 shows the Ar part of the combined systems in terms of the radial atom distribution. The differences between quantum LDA and Vlasov-LDA structures are dramatic for the small Ar matrices. They converge to each other with increasing system size, similarly to the convergence observed in the case of Na properties (Figure 2). The difference is again due to the rigidity of the fixed Gaussian electron distribution for Vlasov-LDA. This exaggerates core repulsion and diminishes dipole attraction. Moreover, we are missing the long range Van-der-Waals attraction (see figure 1). The pressure from the outside shells and the increasing dipole attraction from the far shells produce then the compression towards the quantum mechanical (and thus more realistic) structures. The example demonstrates the limitations of the test-particle method. The smooth Gaussian folding implied in the test-particle representation was perfectly suited for the soft ionic pseudo-potentials of a free metal cluster (and the more so for the jellium approach to a free cluster). But the inherent rigidity of the electronic test-particle distribution becomes a hindrance in connection with steep potentials as they appear here in terms of the repulsive Ar cores. The Vlasov-LDA is certainly not appropriate for detailed studies of subtle binding effects. We find, however, that the structures for larger matrices come out sufficiently well to provide a laboratory for dynamical studies in the non-linear

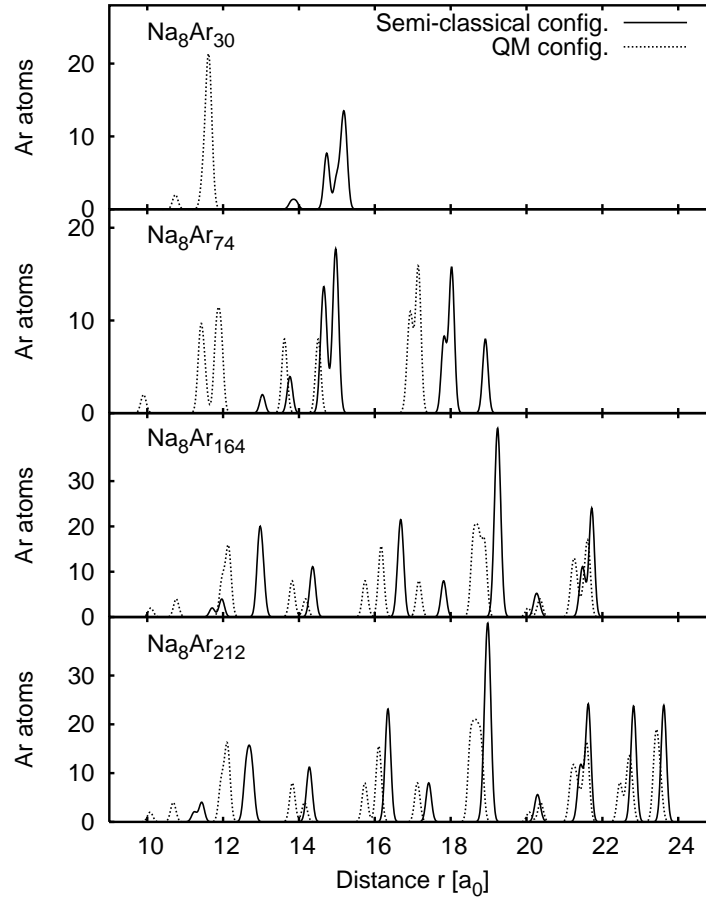


Fig. 3 The distribution of radial shell in Ar matrices of different sizes for Vlasov-LDA and for a fully quantum mechanical treatment.

domain	excitation energy
linear	0.3 eV
semi-linear	4.1 eV
non-linear	13.5 eV

Table 6 Excitation energies for different domains.

regime. Remember that VUU versus Vlasov-LDA is presently the only way to estimate microscopically the effect of dynamical electron correlations on the resonance excitations.

5.2 Dynamics

In order to explore the basic dynamical properties, we employ the most simple excitation mechanism of an instantaneous boost, as explained in section 3.3. It has only one parameter, the boost strength, which allows to scan the various dynamical regimes. We pick a typical strength for each regime as listed in table 6 and characterized by the initial excitation energy. To put that in perspective, one may compare it with the typical energies in the system: at the side of the Na cluster we have the ionization potential with $IP \approx 3.5 - 4.5$ eV and the energy of the Mie surface plasmon with $\omega^{(\text{Mie})} \approx 2.6 - 2.9$ eV. At the side

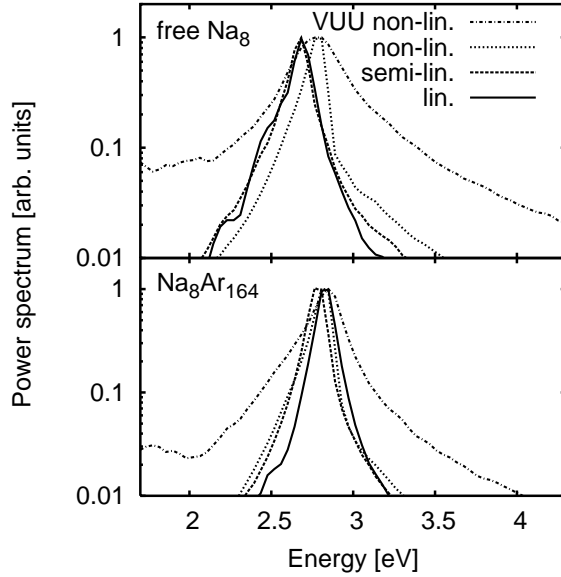


Fig. 4 Results of Vlasov calculations for the power spectrum of the dipole mode along z axis for Na_8 (upper panel) and for $\text{Na}_8@\text{Ar}_{164}$ (lower panel) at different excitation energies. The spectra are normalized to peak maximum at 1 for better comparison. The dipole moment has been recorded for 100 fs.

of the Ar atoms, we have their first electronic excitation and the IP above 20 eV. The linear regime is far below anyone of these scales, the semi-linear just of the same order, and the non-linear regime safely above (multi-plasmon, strong emission).

The spectral properties from Vlasov-LDA (and VUU) are shown in figure 4 in terms of the power spectrum of the dipole mode along z -axis (which corresponds to the approximate symmetry axis of the Na_8 cluster). The general pattern are much similar to previous studies on Na_9^+ [34, 18]. There is a clear resonance peak under any conditions. It is not destroyed by high excitations. These well developed resonance features persist very well also for the embedded cluster. One may even find the pattern somewhat cleaner than for the free cluster. At second glance, one sees trends and developments. There is, e.g., the much larger width in case of VUU which is obviously generated by the electron-electron collisions. We will now work out the trends in terms of the key features of these simple spectra: the peak position $\omega^{(\text{Mie})}$ and the width as full width at half maximum (FWHM).

Figure 5 shows these basic features in case of the system Na_8Ar_n ($n < 212$) for quantum mechanical calculations, Vlasov-LDA, and VUU. The peak frequencies (two lower panels) depend only very weakly on the Ar matrix in all cases. The remaining small trend shows a red shift with increasing matrix size in the quantum mechanical results. That is due to the fact that the additional Ar shells enhance the attractive dipole interaction. The Vlasov results indicate the opposite trend. That is due to the decreasing radius of the inner Ar shell (see figure 3) which gives more weight to the increasing core repulsion. The changes with increasing excitation energy differ. The quantum mechanical results show a sizeable and systematically increasing blue-shift. It can be explained by the increasing ionization which, in turn, deepens the binding potential and thus increases the restoring force for the dipole oscillations [33]. The same trend is hinted in the Vlasov results for the free Na_8 shown in the upper panel of figure 4. But the Vlasov results for the embedded cluster (middle panel of figure 5) behave differently in that the step from the linear to the semi-linear regime shows a tiny (or no) red shift instead of a blue shift. The reasons for that are not yet fully clear. The step into the non-linear regime then produces the blue-shift. Finally, the step to VUU has negligible effect on the peak position as one would have expected.

The uppermost panel of figure 5 shows the widths of the resonance peaks in the Vlasov cases. The spectral analysis uses a recording time of 100 fs and employs a filtering to avoid artefacts from insufficiently

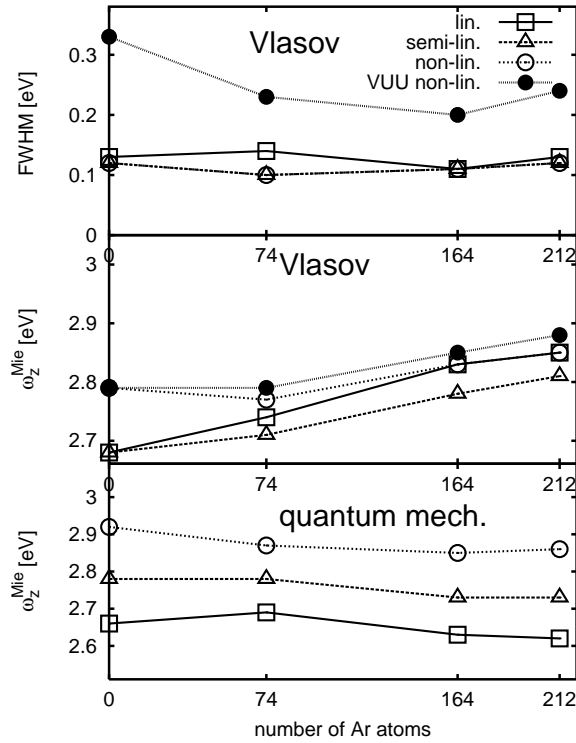


Fig. 5 Position of the Mie plasmon (lower two panels) and its full width at half maximum (FWHM, uppermost panel) for Na_8Ar_n at various excitations as indicated. Lowest panel: quantum mechanical results. Upper two panels: results from Vlasov-LDA (or VUU, respectively).

relaxed signals [35]. This sets the energy resolution of the analysis to 0.1 eV. The width of the Vlasov results is hidden in the resolution except for the non-linear case which shows already some enhancement due to a dynamical spreading (through ongoing ionization) of the spectra. However, the collision term in VUU adds a substantial bit of 0.2 eV for free Na_8 and 0.1 eV for the embedded clusters. It is a bit surprising to see a reduction of the width when the matrix is around. This hints at a somewhat more harmonic potential for the embedded cluster. The effect deserves a deeper analysis which, however, goes beyond scope and limits of this paper.

Figure 6 shows the time evolution of ionization (number of emitted electrons) in case of the non-linear excitation. The pattern for quantum-mechanical TDLDA and Vlasov-LDA are similar: there is a steep initial increase from direct electron emission and then a quick bending over to an almost flat trend. The results agree even quantitatively for the free cluster. For the embedded system, on the other hand, the agreement may be just acceptable but is certainly less perfect with Vlasov-LDA showing about half of emission from TDLDA. The reason is that cores of the surrounding Ar atoms build up a narrow potential barrier of about 1 eV height. This barrier reflects in Vlasov-LDA all test particles which do not have sufficient kinetic energy while quantum mechanical electrons in TDLDA can easily tunnel through. More violent excitations produce a larger fraction of faster electrons and will thus diminish that difference. This confirms once again the rule that semi-classical approaches become increasingly valid with increasing excitation energy. The VUU results in figure 6 show a qualitatively different trend. There remains a slope which hints at significant delayed emission of thermalized electrons. The free Na_8 shows the well understood deal: the VUU curve remains below Vlasov-LDA at early times because direct emission is suppressed in favor of internal thermalization while it crosses the Vlasov line at later times when thermal emission takes over [9]. In case of the embedded cluster, one finds the VUU emission enhanced in all time domains. We see here again a classical effect. The part of thermal emission in VUU is isotropically distributed. The electrons have thus more chances to escape through the saddles between the cores. Moreover, the more

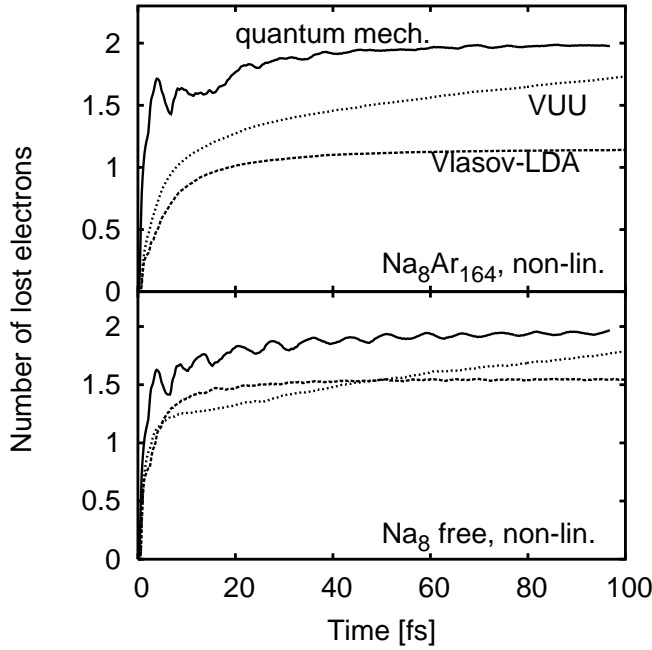


Fig. 6 Time evolution of the number of emitted electrons N_{esc} after strong initial boost with excitation energy 13.5 eV (non-linear regime). Results from quantum mechanical TDLDA, Vlasov-LDA, and VUU are compared. Upper panel: for the system $\text{Na}_8@\text{Ar}_{164}$. Lower panel: for free Na_8 .

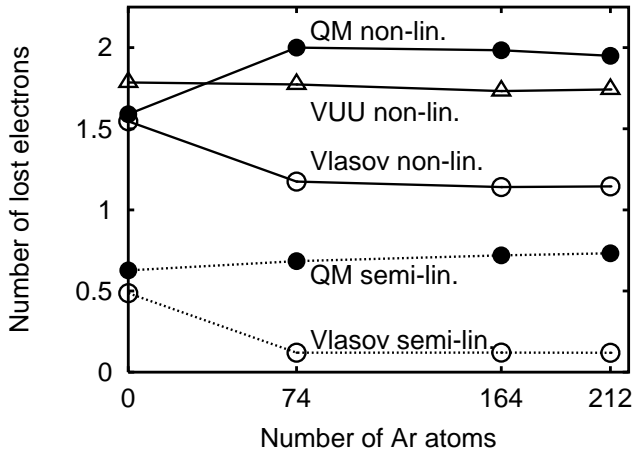


Fig. 7 Final number of emitted electrons N_{esc} after initial boost in semi-linear and non-linear regime (see table 6). Results from quantum mechanical TDLDA, Vlasov-LDA, and VUU are compared.

effective thermalization in VUU allows to fill more systematically the Boltzmann tail of the kinetic energy distribution until some electrons have gathered sufficient energy to surmount the extra barrier.

Figure 7 shows a summary of asymptotic values for ionization for different regimes, methods and system sizes. There is little dependence on the size of the Ar matrix, except for the too small $N_{\text{Ar}} = 30$. Thus we recognize many features from the previous figure. We see again the strong suppression of (direct) emission in Vlasov-LDA. It is even more dramatic in semi linear regime (factor 8 suppression!) because it has a larger fraction of slow electrons which cannot surmount the first Ar barrier. We also find again a systematic trend of enhanced emission in VUU due to its larger contribution from isotropic emission and from the Boltzmann tail. Altogether, the results for electron emission hint that the propagation of slow electrons in the Ar matrix is much different between quantum TDLDA and semi-classical approaches. The latter still provide useful guidelines and presently the only chance to study effects of electron-electron collisions.

One should, however, take care to remain in the regime of strong excitations where slow electrons are less important.

6 Conclusion

In this paper, we have presented a model for the description of the dynamics of an embedded metal cluster (Na) in a rare gas matrix (Ar). The model employs a microscopic description of three basic ingredients: cluster valence electrons, cluster ionic cores, and raregas atoms. The cluster electrons are treated within time-dependent density functional theory (DFT). The cluster ions are treated classically. The raregas atoms are also treated as classical particles together with their dynamical polarizability as intrinsic degree of freedom. This model allows to handle a large variety of dynamical situations at the side of the cluster, including electron emission when non linear excitations are considered. The cluster electrons can be treated at 2 levels of approximation within the realm of DFT: fully quantum mechanical time-dependent local-density approximation (TDLDA) and (semi-classical) Vlasov-LDA. It turns out that both approaches give results which are qualitatively, sometimes even quantitatively, comparable. This holds in the stationary as well as in the dynamical regime. Fully fledged TDLDA reproduces quite well experimental data and previous quantum chemistry approaches. The semi-classical approach also provides an acceptable description for larger raregas matrices, which is to some extent a surprise in view of the subtle energetic balance in these systems.

The semi-classical approach becomes particularly suited when non-linear excitations are considered. It presently provides the simplest and practically only way to deal with dynamical correlations of the cluster electrons. This is achieved by complementing the original Vlasov equation by a Boltzmann-Ühling-Uhlenbeck collision term yielding the Vlasov-Ühling-Uhlenbeck (VUU) model. The collisional correlations induce significant differences between the Vlasov and VUU approaches when a sufficiently large energy is deposited in the system, for free clusters as well as for embedded ones. The test cases considered make it desirable to account for these dynamical correlations also in a quantum mechanical context. This is, however, an extremely difficult task still under development. In the mean time the VUU approach has proven to provide a valuable tool for investigations of the non linear dynamics of simple metal clusters embedded in a rare gas matrix. Further explorations of the various competing phenomena are underway.

Acknowledgments: This work was supported by the DFG, project nr. RE 322/10-1, the french-german exchange program PROCOPE number 04670PG, the CNRS Programme "Matériaux" (CPR-ISMIIR), Institut Universitaire de France, Humboldt foundation and Gay-Lussac price.

References

- [1] U Kreibig and M Vollmer. *Optical Properties of Metal Clusters*, volume 25. Springer Series in Materials Science, 1993.
- [2] H Haberland, editor. *Clusters of Atoms and Molecules 1- Theory, Experiment, and Clusters of Atoms*, volume 52. Springer Series in Chemical Physics, Berlin, 1994.
- [3] W Ekardt, editor. *Metal Clusters*. Wiley, New York, 1999.
- [4] P-G Reinhard and E Suraud. *Introduction to Cluster Dynamics*. Wiley, New York, 2003.
- [5] A A Vlasov. *Many Particle Theory and Its Applications to Plasma*. Gordon & Breach, New York, 1950.
- [6] G F Bertsch and S Das Gupta. *Phys. Rep.*, 160:190, 1988.
- [7] L Feret, E Suraud, F Calvayrac, and P-G Reinhard. *J. Phys. B*, 29:4477, 1996.
- [8] L Plagne and C Guet. *Phys. Rev. A*, 59:4461, 1999.
- [9] A Domsps, P-G Reinhard, and E Suraud. *Ann. Phys. (NY)*, 280:211, 2000.
- [10] E Giglio, P-G Reinhard, and E Suraud. *J. Phys. B*, 34:1253, 2001.
- [11] T Fennel, K-H Meiwes-Broer, and G F Bertsch. *epjd*, ??:?, 2004.
- [12] T Diederich, J Tiggesbümker, and K H Meiwes-Broer. *J. Chem. Phys.*, 116:3263, 2002.
- [13] B Gervais, E Giglio, P-G Reinhard, and E Suraud. *to appear Phys. Rev. A*, 2004.
- [14] B Gervais, E Giglio, P-G Reinhard, and E Suraud. *J. Chem. Phys.*, 121:8466, 2004.

- [15] F Fehrer, P-G Reinhard, E Suraud, B Gervais, and E Giglio. *submitted to Eur. Phys. J. D*, 2004.
- [16] F Dupl e and F Spiegelmann. *J. Chem. Phys.*, 105:1492, 1996.
- [17] A Doms, P L'Eplattenier, P-G Reinhard, and E Suraud. *Ann. Phys. (Leipzig)*, 6:455, 1997.
- [18] E Giglio, P-G Reinhard, and E Suraud. *Ann. Phys. (Leipzig)*, 11:291, 2002.
- [19] E Giglio, P-G Reinhard, and E Suraud. *Phys. Rev. A*, 67:43202, 2003.
- [20] S K ummel, M Brack, and P-G Reinhard. *Euro. Phys. J. D*, 9:149, 1999.
- [21] G Reza Ahmadi, J Alml f, and J Roegen. *Chem. Phys.*, 199:33, 1995.
- [22] Eric Giglio. PhD thesis, Universit Paul Sabatier, Toulouse, 2002.
- [23] M Gross and F Spiegelmann. *J. Chem. Phys.*, 108:4148, 1998.
- [24] M B El Hadj Rhouma, H Berriche, Z B Lakhdar, and F Spiegelman. *J. Chem. Phys.*, 116:1839, 2002.
- [25] F Calvayrac, P-G Reinhard, E Suraud, and C A Ullrich. *Phys. Rep.*, 337:493, 2000.
- [26] M D Feit, J A Fleck, and A Steiger. *J. Comp. Phys.*, 47:412, 1982.
- [27] L Verlet. *Phys. Rev.*, 159:98, 1967.
- [28] K. Husimi. *Prog. Phys. Math. Soc. Japan*, 22:264, 1940.
- [29] E Prugovecki. *Ann. Phys.*, 110:102, 1978.
- [30] K Takahashi. *Prog. Theor. Phys. Supp.*, 98:109, 1989.
- [31] P-G Reinhard and E Suraud. *Ann. Phys. (NY)*, 239:193, 1995.
- [32] P-G Reinhard and E Suraud. *Ann. Phys. (NY)*, 239:216, 1995.
- [33] F Calvayrac, P-G Reinhard, and E Suraud. *Ann. Phys. (NY)*, 255:125, 1997.
- [34] E Giglio, E Suraud, and P-G Reinhard. *Int. J. Phys. C*, 12:1439, 2001.
- [35] W H Press, S A Teukolsky, W T Vetterling, and B P Flannery. *Numerical Recipes*. Cambridge University Press, Cambridge, 1992.